8 Reflection Tomography

8.1 Introduction

The tomographic images up to this point have generally been formed by illuminating an object with some form of energy (x-rays, microwaves, or ultrasound) and measuring the energy that passes through the object to the other side. In the case of straight ray propagation, the measurement can be of either the amplitude or the time of arrival of the received signal; an estimate is then formed of a line integral of the object's attenuation coefficient or refractive index. Even when the energy doesn't travel in a straight line it is often possible to use either algebraic techniques or diffraction tomography to form an image.

Transmission tomography is sometimes not possible because of physical constraints. For example, when ultrasound is used for cardiovascular imaging, the transmitted signal is almost immeasurable because of large impedance discontinuities at tissue–bone and air–tissue interfaces and other attenuation losses. For this reason most medical ultrasonic imaging is done using reflected signals. In the most straightforward approach to reflection imaging with ultrasound, the echoes are recorded as in radar; in medical areas this approach goes by the name of B-scan imaging.

The basic aim of reflection tomography is to construct a quantitative cross-sectional image from reflection data. One nice aspect of this form of imaging, especially in comparison with transmission tomography, is that it is not necessary to encircle the object with transmitters and receivers for gathering the "projection" data; transmission and reception are now done from the same side. The same is of course true of B-scan imaging where a small beam of ultrasonic energy illuminates the object and an image is formed by displaying the reflected signal as a function of time and direction of the beam.

While in transmission tomography it is possible to use both narrow band and broadband signals, in reflection tomography only the latter type is acceptable. As will become evident by the discussion in this chapter, with short pulses (broadband signals) it is possible to form line integrals of some object parameter over lines of constant propagation delays.

Since researchers in reflection tomography are frequently asked to compare B-scan imaging with reflection tomography, in this chapter we will first give a very brief introduction to B-scan imaging, taking great liberties

with conceptual detail; for a rigorous treatment of the subject, the reader is referred to [Fat80]. We will then illustrate how reflection tomography can be carried out with plane wave transducers and some of the fundamental limitations of this type of imaging. Our discussion of reflection tomography with plane wave transducers will include a demonstration of the relationship that exists between reflection tomography and the diffraction tomography formalism presented in Chapter 6. Finally, we will describe how reflection tomographic imaging can be carried out with point transducers producing spherical waves.

8.2 B-Scan Imaging

To explain B-scan imaging, assume that the object inhomogeneities can be modeled by an isotropic scattering function $f(x, y)$, a function of position. In the rest of this chapter, $f(x, y)$ will be referred to as the object reflectivity function. Within certain restrictions, it is a measure of the portion of the local transmitted field that is reflected back toward the receiver. Note that we are taking liberties with rigorous theory, since the scattering process is also a function of the direction of the illumination and the direction in which the reflection is measured. For a more precise analysis the reader is referred to [Fat80].

As shown in Fig. 8.1, a B-scan is a simple example of radar imaging. For illustration, we will assume that within the object the beam is confined to a narrow region along a line as shown in Fig. 8.1(a) and that the amplitude of the field along this line isn't decaying so that it can be written as a function of only one variable, the distance along the line. If the illuminating wave has a very short time duration, there will be a direct mapping between the time at which a portion of the reflected wave is received and the distance into the object.

Mathematically, the received waveform is a convolution of the input waveform, $p_t(t)$, and the object's reflectivity. The incident field can be written as

$$\psi_i(x, y) = p_t\left(t - \frac{x}{c}\right) \qquad \text{for } y = 0 \tag{1}$$

and

$$\psi_i(x, y) = 0 \qquad \text{elsewhere} \tag{2}$$

where c is the propagation speed of the wave. This function models a pulse, $p_t(t)$, propagating down the x-axis, assumed perpendicular to the face of the transducer, with speed c. This is pictorially illustrated in Fig. 8.1(b). At a point (x, y) in the object a portion of the incident field, $\psi_i(x, y)$, will be scattered back toward the transducer. Therefore the amplitude of the scattered

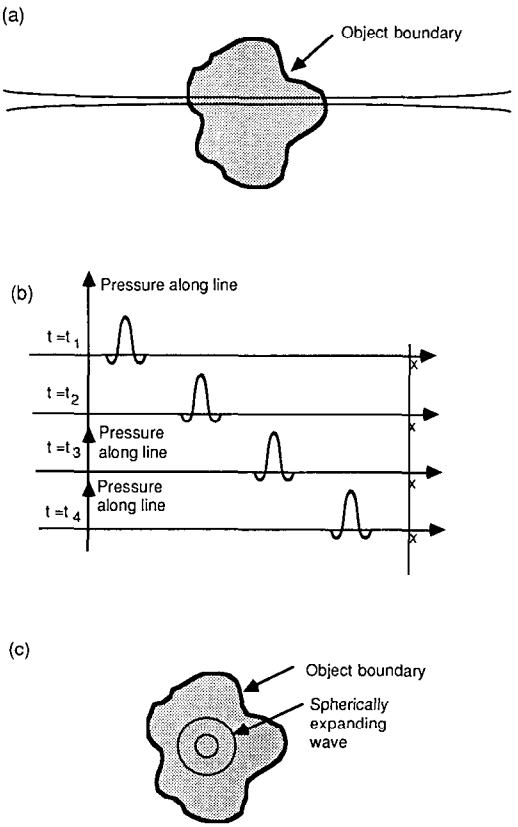

Fig. 8.1: *In B-scan imaging an object is illuminated by a narrow beam of energy. A short (temporal) pulse is transmitted and will propagate through the object. (a) shows a portion of the object illuminated by a "pencil" beam of energy, (b) shows the pulse at different times within the object, and (c) shows the spherically expanding wave caused by a single scatterer within the object.*

field at the scatterer is given approximately by

$$\psi(x, y=0) = f(x, y=0)p_t\left(t-\frac{x}{c}\right). \tag{3}$$

In traveling back to the receiver, the reflected pulse will be delayed by x/c due to the propagation distance involved and attenuated because the reflected field is diverging as depicted in Fig. 8.1(c). To maintain conservation of energy (in two dimensions here) the amplitude attenuation due to spreading is proportional to $1/\sqrt{x}$. That means the energy density will decay as $1/x$ and, when integrated over the boundary of a circle enclosing the scattering site, the total energy outflow will always be the same regardless of the radius of the circle. Thus the field received due to reflection at x is given by

$$\psi_s|_{\text{scattered at } x} = p_t\left(t-\frac{x}{c}-\frac{x}{c}\right) f(x, y=0)\,\frac{1}{\sqrt{x}}. \tag{4}$$

Integrating this with respect to all the reflecting sites along the transmitter

line, the total field at the receiver is given by

$$\psi_s(t) = \int p_t\left(t - 2\frac{x}{c}\right) \frac{f(x, y=0)}{\sqrt{x}}\, dx. \tag{5}$$

With the above expression for the scattered field due to a narrow incident beam it is relatively straightforward to find a reconstruction process for the object's reflectivity. Certainly the simplest approach is to illuminate the object with a pulse, $p_t(t)$, that looks like an impulse. The scattered field can then be approximated by

$$\psi_s(t) = \int \delta\left(t - 2\frac{x}{c}\right) \frac{f(x, y=0)}{\sqrt{x}}\, dx = \sqrt{\frac{c}{2t}}\, f\left(\frac{tc}{2}, y=0\right). \tag{6}$$

This expression shows that there is a direct relation between the scattered field at t and the object's reflectivity at $x = tc/2$. This is shown in Fig. 8.2. With this expression it is easy to see that a reconstruction can be formed using

$$\tilde{f}(x, y=0) = \sqrt{\frac{4x}{c^2}}\, \psi_s\left(\frac{2x}{c}\right) \tag{7}$$

where $\tilde{f}$ is the estimate of the reflectivity function f. The term $4x/c^2$ that multiplies the scattered field is known as time gain compensation and it compensates for the spreading of the fields after they are scattered by the object.

In B-scan imaging, a cross-sectional image of the object's reflectivity variation is mapped out by a combination of scanning the incident beam and measuring the reflected field over a period of time. Recall that in B-scan imaging the object is illuminated by a very narrow beam of energy. Equation (7) then gives an estimate of the object's reflectivity along the line of the object illuminated by the field. To reconstruct the entire object it is then necessary to move the transducer in such a manner that all parts of the object are scanned. There are many ways this can be accomplished, the simplest

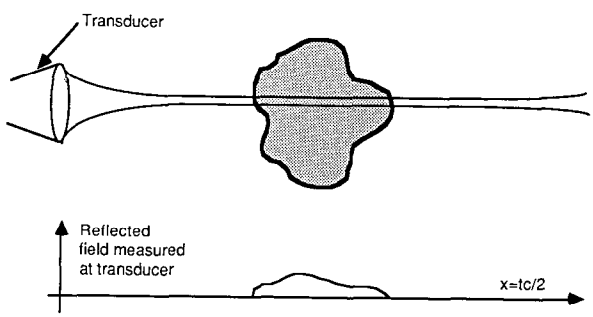

Fig. 8.2: *When an object is illuminated by a pulse there is a direct relationship between the backscattered field and the object's reflectivity along a line.*

being to spin the transducer and let each position of the transducer illuminate one line of a fan. This is the type of scan shown in Fig. 8.3.

Clearly, the resolution in a B-scan image is a function of two parameters: the duration of the incident pulse and the width of the beam. Resolution as determined by the duration of the pulse is often called the range resolution and the resolution controlled by the width of the beam is referred to as the lateral resolution. The range resolution can be found by considering the system response for a single point scatterer. From (5) the field measured at the point (0, 0) due to a single scatterer of "unit strength" at $x = x_0$ will be equal to

$$\psi_s(t) = \frac{p_t\left(t - \frac{2x_0}{c}\right)}{\sqrt{x_0}} . \tag{8}$$

Substituting this in (7), our expression for estimating the reflectivity, we obtain the following form for the image of the object's reflectivity:

$$\tilde{f}(x, y=0) = \sqrt{\frac{4x}{c^2}}\,\psi_s\left(\frac{2x}{c}\right) = \frac{\sqrt{\frac{4x}{c^2}}\,p_t\left(\frac{2x}{c} - \frac{2x_0}{c}\right)}{\sqrt{x_0}} . \tag{9}$$

From this it is easy to see that an incident pulse of width t_p seconds will lead to an estimate that is $t_p c$ units wide.

It is interesting to examine in the frequency domain the process by which the object reflectivity function may be recovered from the measured data. In the simple model described here, the frequency domain techniques can be used by merging the $1/\sqrt{x}$ factor with the reflectivity function; this can be done by defining a modified reflectivity function

$$f'(x, y) = \frac{f(x, y)}{\sqrt{x}} . \tag{10}$$

Now the scattered field at the point (0, 0) can be written as the convolution

$$\psi_s(t) = \int p_t\left(t - 2\frac{x}{c}\right) f'(x, y=0)\, dx \tag{11}$$

and can be expressed in the Fourier domain as

$$\tilde{\psi}_s(\omega) = P_t(\omega) F'\left(2\frac{\omega}{c}, y=0\right) . \tag{12}$$

Given the scattered field in this form it is easy to derive a procedure to estimate the reflectivity of the object. Ideally it is only necessary to divide the

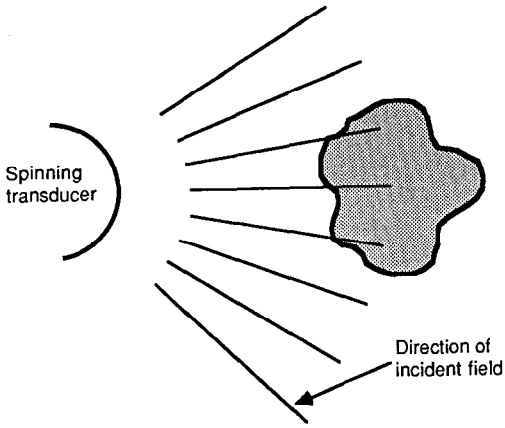

(a)

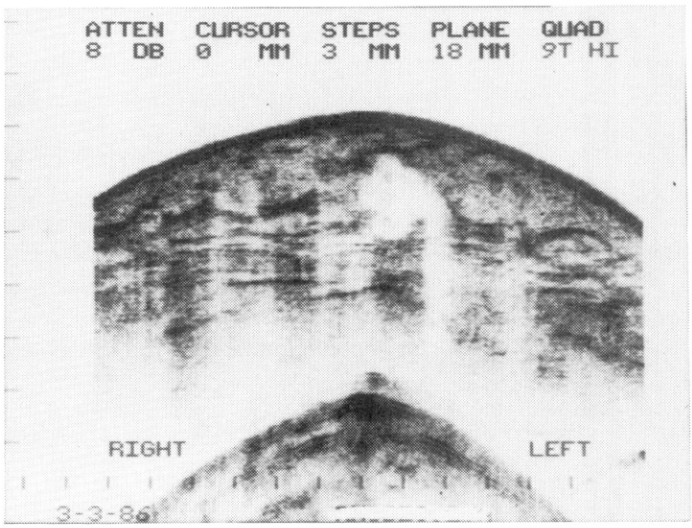

(b)

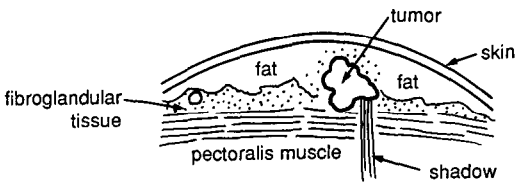

(c)

Fig. 8.3: *Often, in commercial B-scan imaging a focused beam of energy is moved past the object. An image is formed by plotting the received field as a function of time and transducer position. (a) shows this process schematically. (b) is a transverse 7.5-MHz sonogram of a carcinoma in the upper half of the right breast. (This image is courtesy of Valerie P. Jackson, M.D., Associate Professor of Radiology, Indiana University School of Medicine.) (c) is a drawing of the tissue shown in (b). The mass near the center of the sonogram is lobulated, has some irregular borders and low-level internal echoes, and there is an area of posterior shadowing at the medial aspect of the tumor. These findings are compatible with malignancy.*

Fourier transform of the received field by $P_t(\omega)$ to find

$$F'\left(2\frac{\omega}{c}, y=0\right) = \frac{\tilde{\psi}_s(\omega)}{P_t(\omega)}. \tag{13}$$

Unfortunately, in most cases this simple implementation doesn't work because there can be frequencies where $P_t(\omega)$ is equal to zero, which can cause instabilities in the division, especially if there is noise present at those frequencies in the measured data. A more noise insensitive implementation can be obtained via Wiener filtering [Fat80].

8.3 Reflection Tomography

Reflection tomography is based on the measurement of line integrals of the object reflectivity function. Consider a single point transducer illuminating an object with a very wide fan-shaped beam. If the incident field is just an impulse in the time domain, then the received signal at time t represents the total of all reflections at a distance of tc from the transducer. The locus of all points at the same distance from the transmitter/receiver is a circle; thus this mode of reflection tomography measures line integrals over circular arcs. (See Fig. 8.4.) Then by moving the transducer over a plane, or alternatively on a sphere wrapped around the object, it is possible to collect enough line integrals to reconstruct the entire object. This approach to tomographic imaging was described first by Norton and Linzer [Nor79a], [Nor79b].

In principle, reconstruction from such data is similar to the following case that is easier to describe: Instead of using a point transducer, we will use a plane wave transducer. As we will show below, for the two-dimensional case the lines of equal propagation delay now become straight lines through the object and thus the reconstruction algorithms are exactly like those for conventional parallel beam tomography. First, though, we will describe the field generated and received by a plane transducer.

8.3.1 Plane Wave Reflection Transducers

Before deriving a reconstruction procedure using plane waves we first must define what a plane wave transducer measures. In the transmit mode, the field produced by an ideal plane wave transducer when excited by the waveform $p_t(t)$ is equal to

$$\psi_i(x, y, t) = p_t\left(t-\frac{x}{c}\right), \qquad x>0 \tag{14}$$

where we have assumed that the transducer is flush with the plane $x = 0$. Note that the field is only defined in the positive x half space and is a function of one spatial variable.

In the receive mode the situation is slightly more complicated. If $\psi_r(x, y, t)$

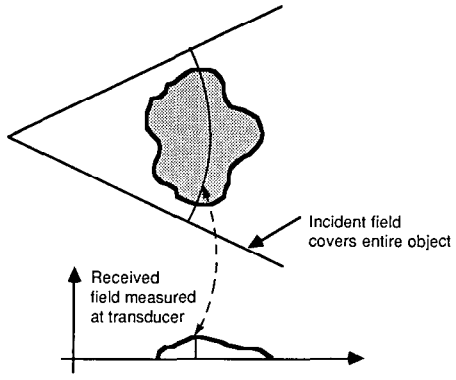

Fig. 8.4: *If a transducer with a wide beam illuminates the object, then it will measure line integrals over circular arcs of the object's reflectivity.*

is the scattered field, the signal generated at the electrical terminals of the transducer is proportional to the integral of this field. We will ignore the constant of proportionality and write the electrical received signal, $p_r(t)$, as

$$p_r(t) = \int \psi_r(0, y, t)\, dy. \tag{15}$$

In order to derive an expression for the received waveform given the field at points distant from the transducer it is necessary to consider how the waves propagate back to the transducer. First assume that there is a line of reflectors at $x = x_0$ that reflect a portion, $f(x = x_0, y)$, of the field. As described above we can write the scattered field at the line $x = x_0$ as the product of the incident field and the reflectivity parameter or

$$\begin{aligned}\psi_s(x=x_0, y, t) &= \psi_i(x=x_0, y, t) f(x=x_0, y) \\ &= p_t\left(t - \frac{x}{c}\right) f(x=x_0, y).\end{aligned} \tag{16}$$

To find the field at the transducer face it is necessary to find the Fourier transform of the field and then propagate each plane wave to the transducer face. This is done by first finding the spatial and temporal Fourier transform of the field at the line of reflectors

$$\tilde{\psi}_s(k_y, \omega) = \int_{-\infty}^{\infty} \int_{-\infty}^{\infty} \psi_s(x=x_0, y, t) e^{-jk_y y} e^{j\omega t}\, dy\, dt. \tag{17}$$

The function $\tilde{\psi}_s(k_y, \omega)$ therefore represents the amplitude of the plane wave propagating with direction vectors $(-\sqrt{(\omega/c)^2 - k_y^2}, k_y)$. It is important to realize that the above equation represents the field along the line as a function of two variables. For any temporal frequency, ω, there is an entire spectrum of plane waves, each with a unique propagation direction.

Recall that we are using the convention for the Fourier transform defined in Chapter 6. Thus the forward transform has a phase factor of $e^{-jk_y y}$ in the spatial domain, as is conventional, while the temporal Fourier transform uses

$e^{+j\omega t}$ for the forward transform. The signs are reversed for the inverse transform.

With this plane wave expansion for the field it is now easy to propagate each plane wave to the transducer face. Consider an arbitrary plane wave

$$\psi(x, y) = e^{j(k_x x + k_y y)} \tag{18}$$

where k_x will be negative indicating a wave traveling back toward the transducer. Using (15), the electrical signal produced is quickly seen to be equal to zero for all plane waves when $k_y \neq 0$. This is due to the fact that

$$\int_{-\infty}^{\infty} e^{jk_y y}\, dy = \delta(k_y). \tag{19}$$

Those plane waves traveling perpendicular to the face of the transducer ($k_y = 0$) will experience a delay due to the propagation distance x_0. In the frequency domain this represents a factor of $e^{j\omega(x_0/c)}$. The electrical response due to a unit amplitude plane wave is then seen to be

$$P_r(\omega, k_y) = \delta(k_y) e^{j\omega(x_0/c)}. \tag{20}$$

By summing each of the plane waves at frequency ω in (17), the total electrical response due to the scattered fields from the plane $x = x_0$ is given by

$$\tilde{P}_r(\omega) = \tilde{\psi}_s(k_y = 0, \omega) e^{j\omega(x_0/c)} \tag{21}$$

or back in the time domain it is simply equal to

$$p_r(t) = \frac{1}{2\pi} \int_{-\infty}^{\infty} \tilde{\psi}_s(k_y = 0, \omega) e^{j\omega(x_0/c)} e^{-j\omega t}\, d\omega. \tag{22}$$

Now substituting (14), (17), and (16) into this expression, the received signal can be written

$$p_r(t) = \frac{1}{2\pi} \int_{-\infty}^{\infty} e^{-j\omega t}\, d\omega \int_{-\infty}^{\infty} \int_{-\infty}^{\infty} \psi_s(x = x_0, y, t') \cdot e^{j\omega(x_0/c)} e^{-jk_y y} e^{j\omega t'}\, dy\, dt' \Big|_{k_y = 0} \tag{23}$$

which is the same as

$$p_r(t) = \frac{1}{2\pi} \int_{-\infty}^{\infty} e^{-j\omega t}\, d\omega \int_{-\infty}^{\infty} \int_{-\infty}^{\infty} \psi_i(x = x_0, y, t') \cdot f(x = x_0, y) e^{j\omega(x_0/c)} e^{j\omega t'}\, dy\, dt' \tag{24}$$

which reduces to

$$p_r(t)=\frac{1}{2\pi}\int_{-\infty}^{\infty} e^{-j\omega t}\,d\omega \int_{-\infty}^{\infty}\int_{-\infty}^{\infty} p_t\left(t'-\frac{x_0}{c}\right) \cdot f(x=x_0, y)e^{j\omega(x_0/c)}e^{j\omega t'}\,dy\,dt'. \quad (25)$$

Interchanging the order of integrations yields

$$p_r(t) = p_t\left(t-2\frac{x_0}{c}\right)\int_{-\infty}^{\infty} f(x=x_0, y)\,dy. \quad (26)$$

The above equation represents the measured signal due to a single line of scatterers at $x = x_0$. Let the total (integrated) reflectivity of the object along the line $x = x_0$ be denoted by $f_1(x_0)$. The received signal for all parts of the object can be written as the sum of each individual line (since we are assuming that the backscattered fields satisfy the Born approximation and thus the system is linear) and the total measured signal can be written

$$p_r(t) = \int_{-\infty}^{\infty} p_t\left(t-2\frac{x}{c}\right) f_1(x)\,dx. \quad (27)$$

This signal is similar to that of B-scan imaging. Like B-scan the transmitted pulse is convolved with the reflectivity of the object but in each case the reflectivity is summed over the portion of the object illuminated by the incident field. In B-scan the object is illuminated by a narrow beam so each portion of the received signal represents a small area of the object. With reflection tomography the beam is very wide and thus each measurement corresponds to a line integral through the object.

Like B-scan imaging the reflectivity of the object can be found by first deconvolving the effects of the incident pulse. If the incident pulse can be approximated by an impulse, then the object's reflectivity over line integrals is equal to

$$f_1(x)=p_r\left(2\frac{x}{c}\right); \quad (28)$$

otherwise a deconvolution must be done and the line integrals recovered using

$$F_1(\omega)=\frac{P_r(\omega)}{P_t\left(2\frac{\omega}{c}\right)} \quad (29)$$

where $F_1(\omega)$, $P_r(\omega)$, and $P_t(\omega)$ represent the Fourier transform of the corresponding time or space domain signal. (In practice, of course, one may have to resort to techniques such as Wiener filtering for implementing the frequency domain inversion.)

The line integral data in the equation above are precisely the information needed to perform a reconstruction using the Fourier Slice Theorem. As described in Chapter 3, the object's reflectivity can be found using the relationship

$$\hat{f}(x, y) = \int_0^{2\pi} \int_{-\infty}^{\infty} S_\theta(\omega) |\omega| e^{j\omega t} \, d\omega \, d\theta \tag{30}$$

where S_θ represents the Fourier transform of the projection data measured with the transducer face at an angle of θ to the horizontal and

$$t = x \cos\theta + y \sin\theta. \tag{31}$$

8.3.2 Reflection Tomography vs. Diffraction Tomography

It is interesting to compare reflection tomography as just described using plane wave transducers to the methods of diffraction tomography presented in Chapter 6. To see the similarities, consider the following imaging experiment. Instead of using a plane wave transducer, let's use a line array to illuminate the object, as shown in Fig. 8.5.

To perform a reflection tomography experiment of the type described in the preceding subsection, we need to be able to generate a plane wave with the array; this can be done easily by applying the same broadband signal $p(t)$ to every transducer in the array. For reception, if we simply add the electrical signals generated by the transducer elements in the array, we will obtain a close approximation to the receiving characteristics of a plane wave transducer.

Now imagine that instead of summing all the received electrical signals, we record each one separately—call each such signal $s(t, y)$. If we take the Fourier transform of each received waveform $s(t, y)$ with respect to time, we obtain

$$S(\omega, y) = \int_{-\infty}^{\infty} s(t, y) e^{j\omega t} \, dt. \tag{32}$$

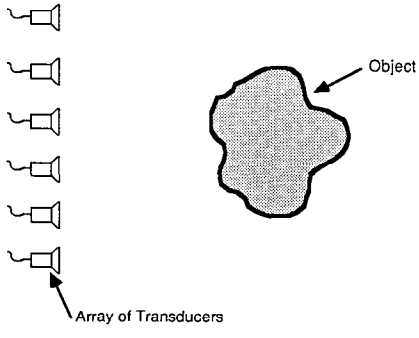

Fig. 8.5: *By using a common signal source and combining all the electrical signals, an array of transducers can be used to generate a plane wave for reflection tomography. However, by recording the information separately for each transducer, they can also be used for the more general form of reflection tomography.*

If the original signal has a spectrum given by

$$P_t(\omega) = \int_{-\infty}^{\infty} p_t(t) e^{j\omega t}\, dt, \tag{33}$$

then the scattered fields can be normalized by dividing the received spectrum by the transmitted spectrum to find

$$S'(\omega, y) = \frac{S(\omega, y)}{P_t(\omega)}. \tag{34}$$

Again, as described before, this represents an idealized approach and in practice a more robust filter must be used.

Because of the normalization at the array element at location y, the data $S'(\omega, y)$ represent a single plane wave component of the scattered field that is at a temporal frequency of ω. If we take a Fourier transform of $S'(\omega, y)$ with respect to the variable y, by using the techniques of Chapter 6 we can derive the following relationship:

$$S'(\omega, k_y) = \int_{-\infty}^{\infty} S'(\omega, y) e^{-jk_y y}\, dy = F(-\sqrt{k_0^2 - k_y^2} - k_0, k_y) \tag{35}$$

which shows that the Fourier transform[1] $S'(\omega, k_y)$ provides us with an estimate of the Fourier transform of the object reflectivity function along a circular arc, as illustrated in Fig. 8.6 for a number of different frequencies.

This means that a cross-sectional image of the object could be reconstructed by rotating the object in front of the array, since via such a rotation we should be able to fill out a "disk with a hole in the center" shaped region in the frequency domain. The reconstruction can be carried out by taking an inverse Fourier transform of this region. Clearly, since the center part of the disk would be missing, the reconstructed image would be a "high pass" version of the actual reflectivity distribution.

Reflection tomography using plane wave transducers, as described in the preceding subsection, is a special case of the more general form presented here. This can be shown as follows: If the signals $s(t, y)$ received by the transducers are simply summed over y, the resulting signal as a function of time represents not only the output from an idealized plane wave receiver but also the Fourier transform of the received field at a spatial frequency of $k_y = 0$. We can, for example, show that the Fourier transform of the summed signal

$$\int_{-\infty}^{\infty} s(t, y)\, dy \tag{36}$$

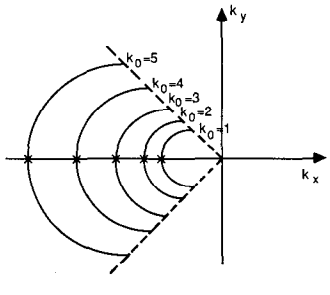

Fig. 8.6: *The Fourier transform of the field received by a plane wave transducer gives samples of the two-dimensional Fourier transform of the object along the line indicated by the cross marks. For each spatial frequency, k_0, the backscattered field gives information along an arc. A plane wave transducer only measures the dc component; thus the measured signal contains information about only one point of each arc. By rotating the transducer around the object a complete reconstruction can be formed.*

[1] Note that the expression defined in (32) represents the received signal, S, as a function of temporal frequency, ω, and spatial position, y, while (35) represents the normalized signal as a function of both spatial (k_y) and temporal (ω) frequency.

is given by

$$\int_{-\infty}^{\infty}\int_{-\infty}^{\infty} s(t, y)\, dy\, e^{j\omega t}\, dt = P_t(\omega)[F(-\sqrt{k_0^2 - k_y^2} - k_0, k_y)]_{k_y=0} \tag{37}$$

$$= P_t(\omega)F(-2k_0, 0) \tag{38}$$

$$= P_t(\omega)F\left(-2\frac{\omega}{c}, 0\right) \tag{39}$$

which shows that the Fourier transform of the summed signal gives the Fourier transform of the object along the straight lines as given by

$$F\left(-2\frac{\omega}{c}, 0\right) \qquad \text{for } 0 < \omega < \infty. \tag{40}$$

These data points are shown as crosses in Fig. 8.6.

8.3.3 Reflection Tomography Limits

Limitations of reflection tomography are similar to those of transmission tomography described in Chapter 6. In both cases the interactions of the field and the object are modeled using first-order approximations.

Barry Roberts at Purdue University performed a number of simulations to study the limitations of plane wave reflection tomography. The simulations were done to model an ideal plane wave tomography experiment using a large bandwidth and a very large transducer.

The data used to study the quality of the reflection tomographic algorithms were calculated by assuming that the incident field is the sum of a number of discrete frequencies between K_{0L} and K_{0H}. For each frequency, a unit amplitude plane wave was scattered off a cylinder with a constant refractive index. The backscattered field was then integrated over the receiver line to find $S(\omega, k_y = 0)$.

Fig. 8.7 shows the reflection tomographic reconstructions using an ideal transducer with infinite frequency response. Even in this case it is not possible to measure the object's response for a wave at $k_0 = 0$ (temporal frequency is zero). Thus the value for the $k_0 = 0$ term was interpolated and there was some shift in the dc value of the reconstruction.

The reconstructions shown here are similar to the ones shown in Chapter 6 for the Born approximation in the forward direction. For small objects and refractive indexes the reflection reconstructions are good, but for large objects the high frequency part of the reconstruction is distorted. This is because the high frequency components, or those with the shortest wavelengths, are first to undergo a 180° phase change. Thus in the $10\lambda_c$ reconstructions the edges are distorted until finally, as the refractive index

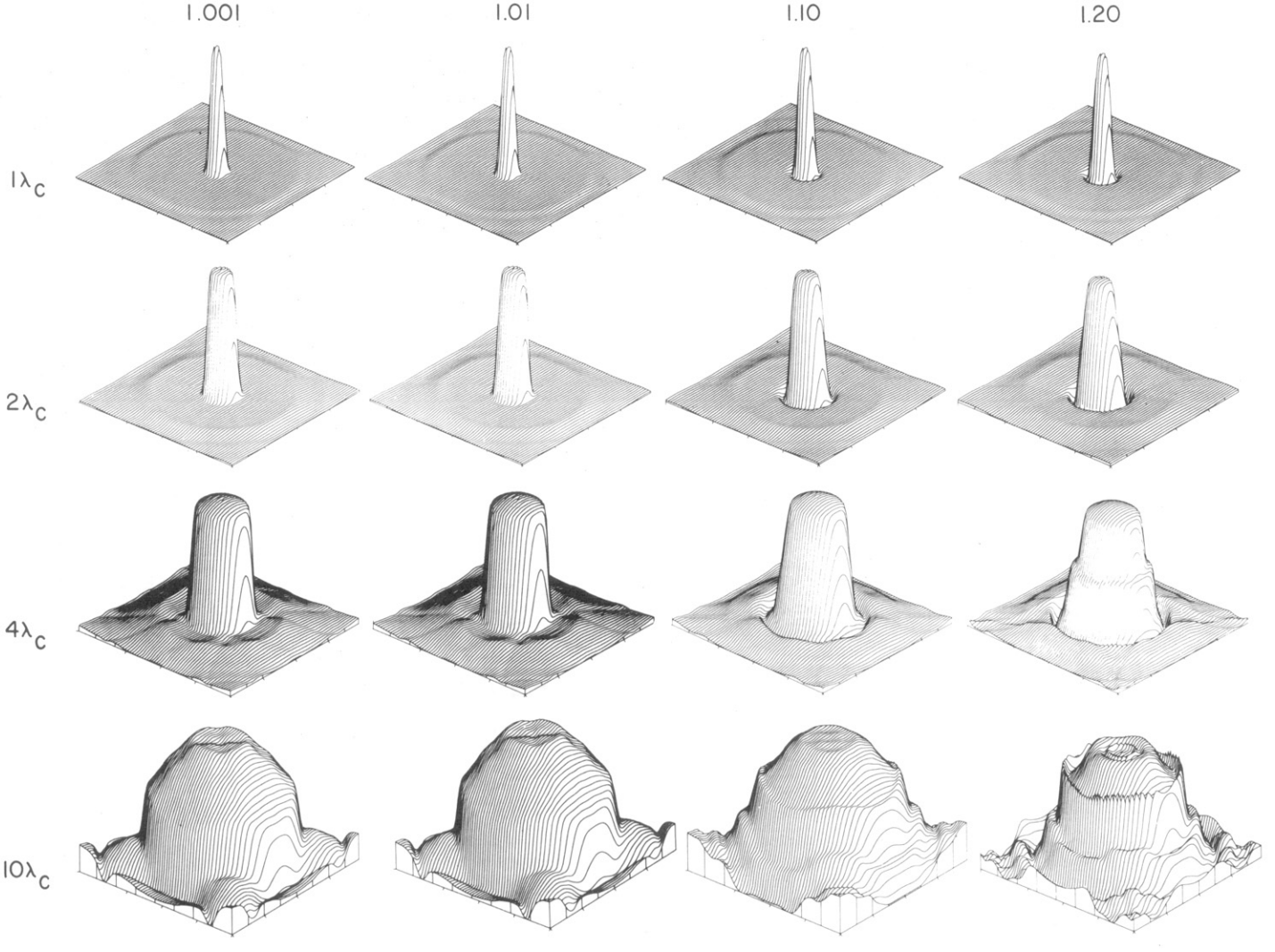

Fig. 8.7: *Plane wave reflection reconstruction of 16 cylinders with a refractive index between 1.001 and 1.20 and radius between 1 and 10λ_c are shown here. The incident field includes wavelengths between (20/32)λ_c and (20/8)λ_c and represents nearly an ideal case since very low frequencies (high wavelengths) are included. The dc component of these reconstructions was calculated by interpolation. (Courtesy of Barry Roberts, Purdue University, Lafayette, IN.)*

approaches 1.20, there are some small high frequency ripples. (λ_c refers to the wavelength at the center frequency of the transducer bandwidth.)

Using a more practical frequency range the reconstructions shown in Fig. 8.8 are obtained. Here the data simulate what might be measured with a transducer with a center frequency of 1 MHz and a bandwidth of 1.2 MHz. As would be expected, the reconstructions aren't as good as those shown in Fig. 8.7 because some of the low and high frequency information about the object is missing. Thus there is very little information in the reconstructions other than the location of the edges of the cylinders. The average refractive index of each cylinder isn't reconstructed because that is contained in the low frequencies.

A big problem with reflection tomography is that it doesn't provide information about the object at low frequencies. To a certain extent this problem can be rectified by extrapolating the measured object spectrum into the low frequency band where the information is missing. A popular algorithm for such an extrapolation is the Gerchberg–Papoulis algorithm [Ger74], [Pap75].

The Gerchberg–Papoulis algorithm is an iterative procedure to combine information about the Fourier transform of a function (as might be produced by a reflection tomography experiment) with independent space domain constraints. Typically, the spatial constraint might be the known support of the object or the fact that it is always positive.

Assume that a reflection tomography experiment has yielded $F_0(u, v)$ as an estimate of the Fourier transform of an object's cross section; its inverse Fourier transform $f_0(x, y)$ is then the image that would be the result of the experiment. From the preceding arguments $F_0(u, v)$ is known in a doughnut-shaped region of the (u, v) space; we will denote this region by D_f. In general, the experiment itself wouldn't reveal anything about the object outside the doughnut-shaped region. If $f(x, y)$ denotes the true cross section and $F(u, v)$ the corresponding transform, we can write

$$F(u, v) = \begin{cases} F_0(u, v) & (u, v) \text{ in } D_f \\ ? & \text{elsewhere.} \end{cases} \tag{41}$$

We will invoke the constraint that the object is known to be spatially limited:

$$f(x, y) = \begin{cases} ? & (x, y) \text{ in } D_s \\ 0 & \text{elsewhere} \end{cases} \tag{42}$$

where we have used D_s to denote the maximum a priori known object size.

Typically, the inverse Fourier transform of the known data $F_0(u, v)$ will lead to a reconstruction that is not spatially limited. The goal of the Gerchberg–Papoulis algorithm is to find a reconstruction $f^*(x, y)$ that satisfies the space constraint and whose Fourier transform $F^*(u, v)$ is equal to that measured by reflection tomography in region D_f. We will now describe how this algorithm can be implemented.

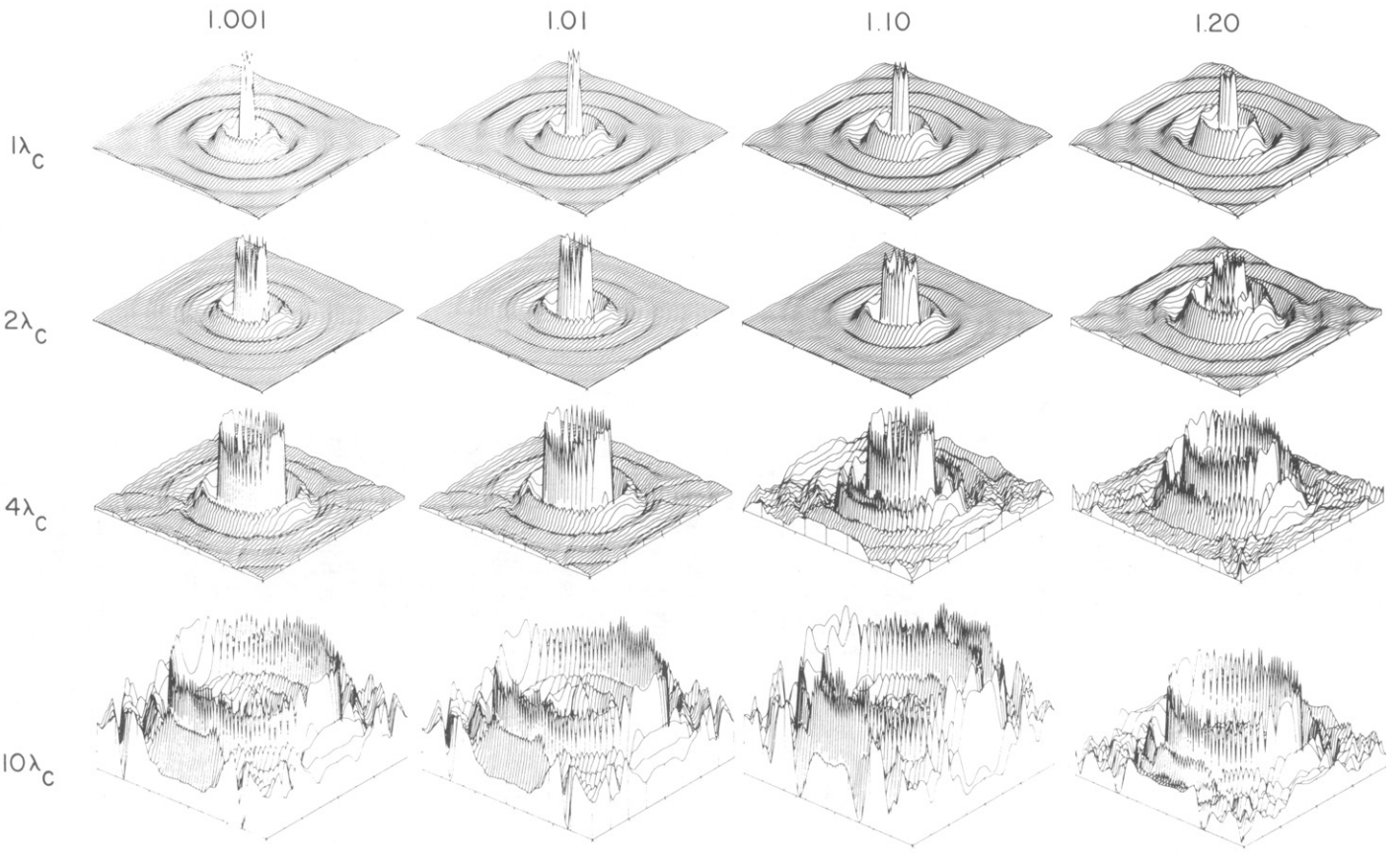

Fig. 8.8: *Reconstructions similar to those in Fig. 8.7 are shown here with more realistic frequency limits. In this case the transducer illuminated the object with a pulse at a center frequency of 1 MHz and a bandwidth of 1.2 MHz. The radius of the cylinders is shown as a function of the wavelength of the center frequency (1 MHz). (Courtesy of Barry Roberts, Purdue University, Lafayette, IN.)*

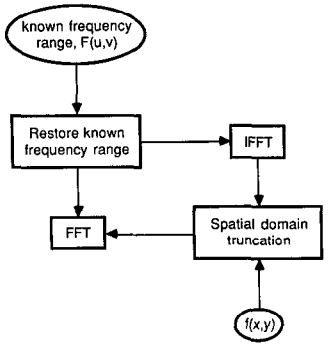

Fig. 8.9: *In the Gerchberg–Papoulis algorithm an estimate of a portion of the object's Fourier transform is combined with knowledge of its spatial support. The method iterates until an estimate of the object is found that is consistent with the known frequency domain data and the spatial extant of the object. (From [Rob85].)*

Given an initial estimate $F_0(u, v)$, a better estimate of the object is found by finding the inverse Fourier transform of $F_0(u, v)$ and setting the first iteration to be

$$f_1(x, y) = \begin{cases} \text{IFT } \{F_0(u, v)\} & (x, y) \text{ in } D_s \\ 0 & \text{elsewhere.} \end{cases} \tag{43}$$

The next iteration is obtained by Fourier transforming $f_1(x, y)$ and then constructing a composite function in the frequency domain as follows:

$$F_1(u, v) = \begin{cases} F_0(u, v) & (u, v) \text{ in } D_f \\ \text{FT } \{f_1(x, y)\} & \text{elsewhere} \end{cases} \tag{44}$$

(FT = Fourier transform). We now construct the next iterate $f_2(x, y)$, which is an improvement over $f_1(x, y)$, by first inverse Fourier transforming $F_1(u, v)$ and setting to zero any values that are outside the region D_s. This iterative process may be continued to yield f_3, f_4, and so on, until the difference between two successive approximations is below a prespecified bound. This is shown schematically in Fig. 8.9.

The result of applying 150 iterations of the Gerchberg–Papoulis algorithm to the reconstructions of Fig. 8.7 is shown in Fig. 8.10. The reader is referred to [Rob85] for further details on the application of this algorithm to reflection tomography.

8.4 Reflection Tomography with Point Transmitter/Receivers

As mentioned before, reflection tomography using point transducers leads to line integrals of the object reflectivity function over circular arcs. We will now show that it is possible to reconstruct the reflectivity function by carrying out a backprojection over circular arcs. The derivation here will follow that of Norton and Linzer [Nor79a], [Nor79b]. A more rigorous derivation can be found in [Nor81].

8.4.1. Reconstruction Algorithms

Assume that the object is illuminated by spherical waves produced by a point source at $\vec{r} = (0, 0)$. Such a field can be expressed as

$$\psi_i(t, \vec{r}) = p_t\left(t - \frac{|\vec{r}|}{c}\right). \tag{45}$$

The field scattered by a single scattering site at position $\vec{r}$ can be expressed as

$$\psi_s(t, \vec{r}) = f(\vec{r}) p_t\left(t - \frac{|\vec{r}|}{c}\right). \tag{46}$$

(For simplicity we will continue to assume that both the illuminating field and

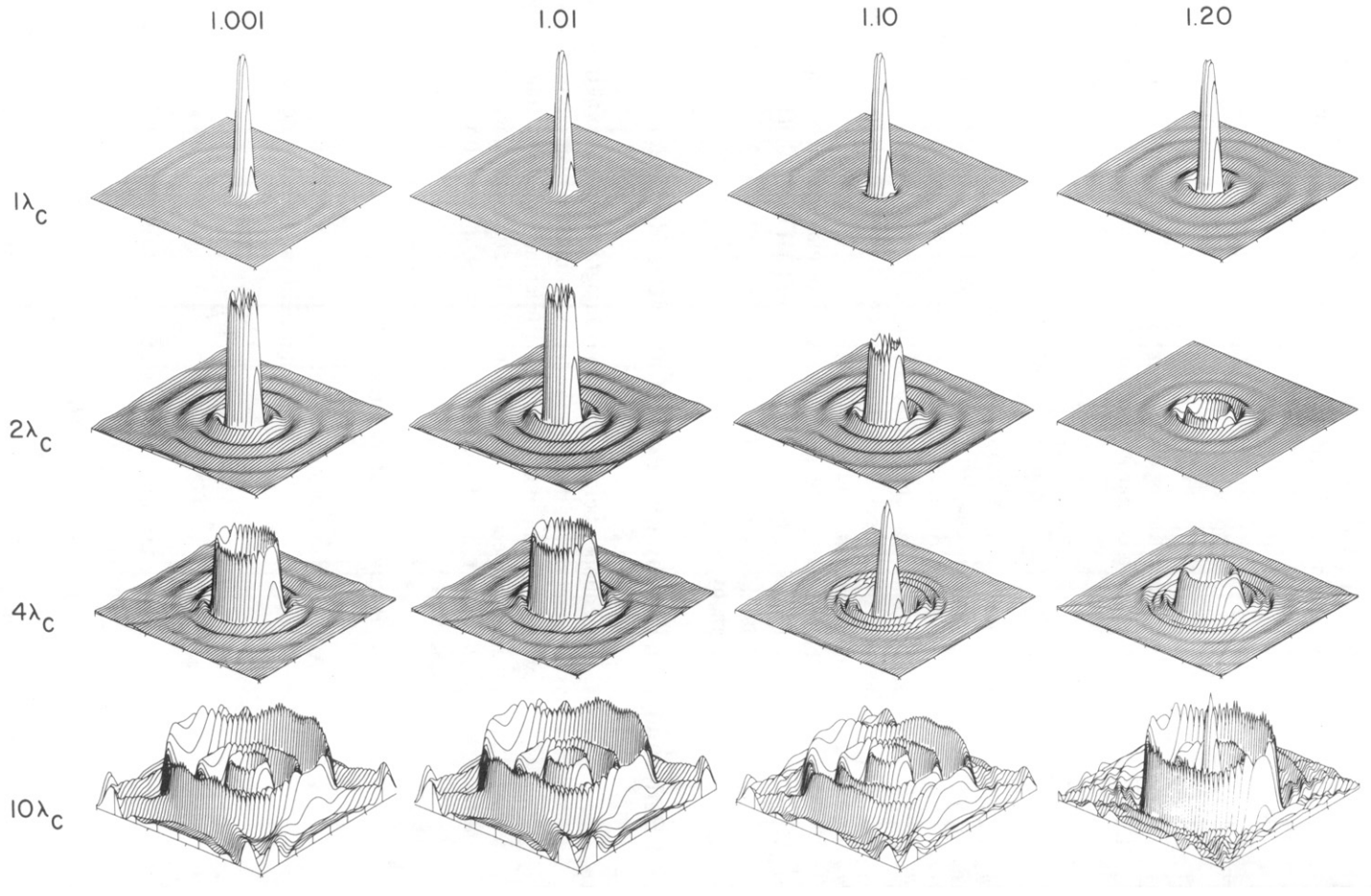

Fig. 8.10: *The Gerchberg–Papoulis algorithm is used on the reconstructions of Fig. 8.8 to produce more accurate reconstructions. (Courtesy of Barry Roberts, Purdue University, Lafayette, IN.)*

the object are two dimensional.) Since we are operating in the reflection mode, we use the same point transducer to record whatever scattered fields arrive at that site. Since the illuminating field is omnidirectional, the scattered field measured at the point transducer will be given by the following integration over the half space in front of the transducer:

$$\psi_s(t) = \int f(\vec{r}) p_t\left(t - 2\frac{|\vec{r}|}{c}\right) |\vec{r}|^{-1/2}\, d\vec{r}. \tag{47}$$

The reason for the factor $|\vec{r}|^{-1/2}$ is the same as that for the factor $1/\sqrt{x}$ in our discussion on B-scan imaging and the extra factor of $|\vec{r}|/c$ represents the propagation delay from the point scatterer back to the transducer. Again, as was done for the B-scan case, the effect of the transmitted pulse can now be deconvolved, at least in principle, and the following estimate for the line integral of the reflection data, $g(r)$, can be made:

$$g(r) = \text{IFT}\left[\frac{\text{FT}\{\psi_s(t)\}}{\text{FT}\{p_t(t)\}}\right] r^{1/2} \tag{48}$$

where FT{ } indicates a Fourier transform with respect to t and IFT{ } represents the corresponding inverse Fourier transform. The function $g(r)$ is therefore a measure of line integrals through the object where the variable r indicates the distance from the transducer to the measurement arc. The variable r is related to t by $r = ct/2$, where c is the velocity of propagation in the medium.

This type of reflection imaging makes a number of assumptions. Most importantly, for (47) to be valid it is necessary for the Born approximation to hold. This means that not only must the scattered fields be small compared to the incident fields, but the absorption and velocity change of the field must also be small. Second, the scatterers in the object must be isotropic scatterers so that the field scattered by any point is identical no matter from what direction the incident field arrives.

These line integrals of reflectivity can be measured from different directions by surrounding the object with a ring of point transducers. The line integrals measured by different transducers can be labeled as $g_\phi(r)$, ϕ indicating the "direction" (and location) of the point transducer in the ring, as shown in Fig. 8.11.

By analogy with the straight ray case it seems appropriate to form an image of the object by first filtering each line integral and then backprojecting the data over the same lines on which they were measured. Because the backprojection operation is linear we can ignore the filter function for now and derive a point spread function for the backprojection operator over circular arcs. With this information an optimum filter function $h(r)$ will then be derived that looks surprisingly like that used in straight ray tomography.

For now assume that the line integral data, $g_\phi(r)$, are filtered by the

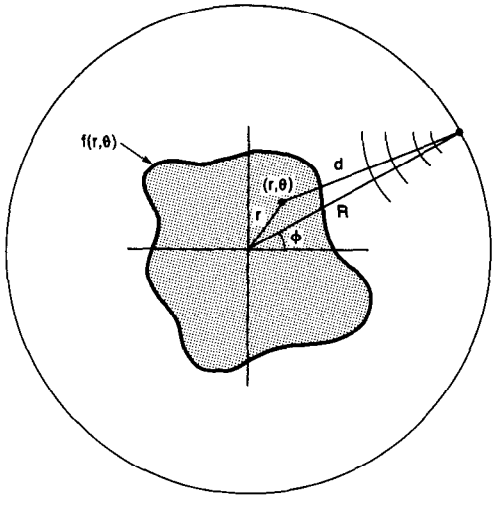

Fig. 8.11: *In reflection tomography with a point source the transducer rotates around the object at a radius of R and its position is indicated by (R, φ). The measured signal, $g_\phi(r)$, represents line integrals over circular arcs centered at the transducer.*

function $h(r)$ to find

$$g'_\phi(r) = g_\phi(r) * h(r). \tag{49}$$

The backprojection operation over circular arcs can now be written

$$\hat{f}(r, \phi) = \frac{1}{2\pi} \int_0^{2\pi} g'_\phi [\rho(\phi; r, \theta)] \, d\phi \tag{50}$$

where the distance from the transducer at (R, ϕ) to the reconstruction point at (r, θ) is given by

$$\rho(\phi; r, \theta) = \sqrt{R^2 + r^2 - 2Rr \cos(\theta - \phi)} \, . \tag{51}$$

In order to determine $h(r)$ we will now use (50) to reconstruct the image of a single scatterer; this image is called the point spread function of the backprojection process. For a single scatterer at (r, θ_0) the filtered projection is

$$p_{r,\phi}(r - \rho(\phi; r, \theta)) = p_t(r - \rho(\phi; r, \theta)) * h(r) \tag{52}$$

since $p_{r,\phi}$, p_t, and h are all functions of distance. The function $p_{r,\phi}$ represents a filtered version of the transmitted pulse; in an actual system the filter could be applied before the pulse is transmitted so that simple backprojection would produce an ideal reconstruction.

The reconstruction image is then given by

$$\hat{f}(r, \theta) = \frac{1}{2\pi} \int_0^{2\pi} p_{r,\phi}[\rho(\phi; r, \theta) - \rho(\phi; r_0, \theta_0)] \, d\phi. \tag{53}$$

We want $h(r)$ to be such that $\hat{f}$ is as close to a Dirac delta function as possible. In order to find an optimum $h(r)$ in this manner, a number of approximations are necessary. First we expand the argument for $g'_\phi(r)$ in the equation above

$$\rho(\phi;\, r,\, \theta)-\rho(\phi;\, r_0,\, \theta_0)=[R^2+r^2-2Rr\cos(\theta-\phi)]^{1/2} - [R^2+r_0^2-2Rr_0\cos(\theta_0-\phi)]^{1/2}. \quad (54)$$

Each term on the right-hand side can be expanded by using

$$\sqrt{1+x}=1+\frac{1}{2}x-\frac{1}{8}x^2+\frac{1}{48}x^3+\cdots. \quad (55)$$

We will now assume that the measurement circle is large enough so that $(r/R)^2$ and $(r_0/R)^2$ are both sufficiently small; as a consequence, the terms that contain powers of r/R and r_0/R_0 greater than 2 can be dropped. Therefore the difference in distances between the two points can be written as

$$\rho(\phi;\, r,\, \theta)-\rho(\phi;\, r_0,\, \theta_0)\approx -r\cos(\theta-\phi)+r_0\cos(\theta_0-\phi)+\frac{r^2-r_0^2}{4R} - \frac{r^2}{4R}\cos 2(\theta-\phi)+\frac{r_0^2}{4R}\cos 2(\theta_0-\phi). \quad (56)$$

This can be further simplified to

$$\rho(\phi;\, r,\, \theta)-\rho(\phi;\, r_0,\, \theta_0)=X\cos(\phi-Y)+\gamma_1+\gamma_2\cos 2(\phi-\alpha) \quad (57)$$

where

$$X=\sqrt{r_0^2+r^2-2r_0r\cos(\theta-\theta_0)} \quad (58)$$

$$\tan Y=\frac{r_0\sin\theta_0-r\sin\theta}{r_0\cos\theta_0-r\cos\theta} \quad (59)$$

$$\gamma_1=\frac{1}{4R}(r^2-r_0^2) \quad (60)$$

$$\gamma_2=\frac{1}{4R}[r_0^4+r^4-2r^2r_0^2\cos 2(\theta-\theta_0)]^{1/2} \quad (61)$$

$$\tan\alpha=\frac{r_0^2\sin 2\theta_0-r^2\sin 2\theta}{r_0^2\cos 2\theta_0-r^2\cos 2\theta}. \quad (62)$$

Now (53) can be written as

$$\hat{f}(r,\, \theta)=\frac{1}{2\pi}\int_0^{2\pi} p_{r,\phi}[X\cos(\phi-Y)+\gamma_1+\gamma_2\cos 2(\phi-\alpha)]\, d\phi. \quad (63)$$

Let $P_{r,\phi}(\omega)$ denote the Fourier transform of the line integral $p_{r,\phi}(r)$, that is,

$$p_{r,\phi}(r)=\frac{1}{2\pi}\int_{-\infty}^{\infty} P_{r,\phi}(\omega)e^{j\omega r}\,d\omega. \tag{64}$$

In terms of the Fourier transform of the filtered line integral data, $\hat{f}$ can be written as

$$\hat{f}(r,\theta)=\int_0^{2\pi} d\phi \int_{-\infty}^{\infty} d\omega\, P_{r,\phi}(\omega)e^{j\omega[\gamma_1+\gamma_2\cos 2(\phi-\alpha)]}e^{j\omega X\cos(\phi-Y)}. \tag{65}$$

This result can be further simplified if the measurement radius, R, is large compared to both the radii r and r_0 and the distance between the point scatterer and the point of interest in the reconstruction. With this assumption it can be shown that both γ_1 and γ_2 are small and the point spread function can be written [Nor79a]

$$\hat{f}(r,\theta)=\frac{1}{2\pi}\int_0^{2\pi} d\phi \int_{-\infty}^{\infty} d\omega\, P_{r,\phi}(\omega)e^{j\omega X\cos(\phi-Y)}. \tag{66}$$

When the scattering center is located at the origin, the point spread function is obtained by using

$$\rho(\phi;\, r,\, \theta)-\rho(\phi;\, 0,\, 0)=r\cos(\phi-\theta) \tag{67}$$

and is given by

$$\hat{f}(r,\theta)=\frac{1}{2\pi}\int_0^{2\pi} d\phi \int_{-\infty}^{\infty} d\omega\, P_{r,\phi}(\omega)e^{j\omega r\cos(\phi-\theta)}. \tag{68}$$

This result can be further simplified by using the Bessell identity

$$J_0(r)=\frac{1}{2\pi}\int_0^{2\pi} d\phi\, e^{jr\cos(\phi-q)} \tag{69}$$

(where q is an arbitrary constant) and rearranging the order of integration to find

$$\hat{f}(r,\theta)=\int_{-\infty}^{\infty} P_{r,\phi}(\omega)J_0(\omega r)\,d\omega \tag{70}$$

where we have assumed that $P_{r,\phi}$ is independent of ϕ for a scatterer located at the origin.

With an expression for the point spread function it is possible to set it equal to a delta function and solve for the optimum filter function. The optimum

impulse response $\delta(x, y)$ can be written in polar form as

$$\delta(x, y) = \frac{\delta(r)}{|r|\pi} \tag{71}$$

when the scattering center is located at the origin. The optimum filter function is then found by noting the identity

$$\int_0^\infty J_0(r\omega)\omega \, d\omega = \frac{1}{r}\,\delta(r). \tag{72}$$

Rewriting the point spread function to put it into this form and using the fact that $J_0(\cdot)$ is an even function, it is easy to show that the optimum form for the filtered line integral data is

$$P_{r,\phi}(\omega) = \frac{|\omega|}{2\pi}\,. \tag{73}$$

Since $P_{r,\phi}(\omega)$ is equal to

$$P_{r,\phi}(\omega) = H(\omega)P_{t,\phi}(\omega) \tag{74}$$

the optimum point spread response will occur when the product of the Fourier transform of the transmitted pulse and the reconstruction filter is equal to

$$P_{t,\phi}(\omega)H(\omega) = \frac{|\omega|}{2\pi}\,. \tag{75}$$

If the spectrum of the transmitted pulse is equal to

$$P_{t,\phi}(\omega) = \frac{|\omega|}{2\pi}\,, \tag{76}$$

then backprojection, without any additional filtering, will produce the optimum reconstruction.

This filter function is not practical since it emphasizes the high frequencies. Generally, a more realistic filter will be a low pass filtered version of the optimum filter or

$$H(\omega) = \frac{|\omega|}{2\pi} \qquad \text{for } |\omega| < \omega_c \tag{77}$$

$$H(\omega) = 0 \qquad \text{elsewhere.} \tag{78}$$

Using this filter function the point spread function for the reconstruction procedure becomes

$$\hat{f}(r, \theta) = \frac{\omega_c J_1(2\omega_c X)}{X}\,. \tag{79}$$

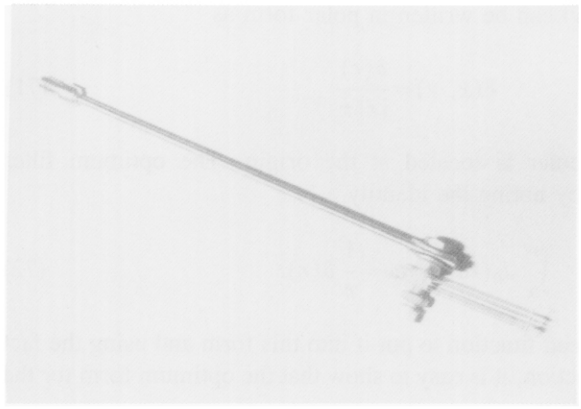

(a)

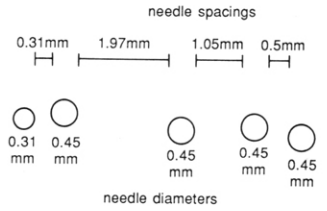

(b)

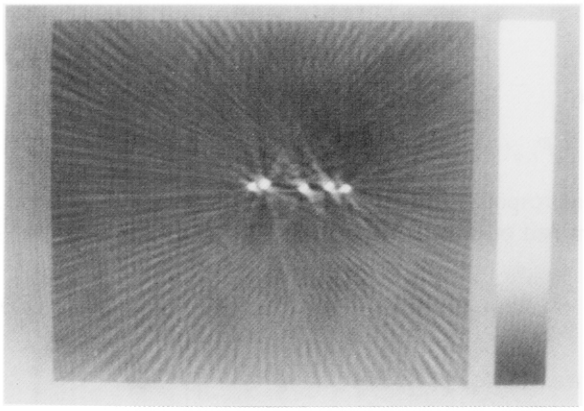

(c)

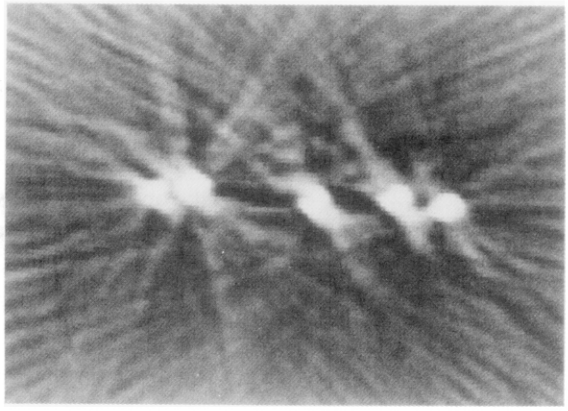

(d)

Fig. 8.12: *A broadband reflection tomogram of five needles is shown here. In this experiment a pixel size of 0.1 mm, an image size of 300 × 300 pixels, 120 projections, and 256 samples per projection were used. This figure shows (a) the needle array, (b) a diagram of a needle array cross section showing sizes and spacing, (c) a reflection tomogram of an array cross section, and (d) a magnified (zoomed) view of (c). (These images are courtesy of Kris Dines, XDATA Corp., Indianapolis, IN, based on work sponsored by National Institute of Health Grant #1 R43 CA36673-01.)*

Thus the width of the main sidelobe is given by

$$X_0 \approx 0.30 \frac{2\pi}{\omega_c} = 0.30\lambda_c \tag{80}$$

where λ_c is the wavelength of the wave corresponding to the cutoff frequency ω_c.

The reconstruction procedure can be summarized as follows. First use (48) to transform the measured data into measures of line integrals over circular arcs. The data should then be filtered with (49) and then backprojected using (50).

8.4.2 Experimental Results

We would now like to mention experimental results obtained by Kris Dines of XDATA Corporation, Indianapolis, IN. In these reconstructions the

distance between the point transducer and the object was large enough so that the line integrals over circular arcs could be approximated as straight lines; the transducer was 200 mm from the center of a 10-mm object. By assuming the integration path can be approximated by a straight line the maximum error in the integration path is 0.25 mm.

The reconstruction of Fig. 8.12(c) shows the resolution that is possible with this method. The five needles suspended in water represent nearly the ideal case since there is no phase shift caused by the object. More experimental work is needed to show the viability of this method in human patients.

8.5 Bibliographic Notes

There is a large body of work that describes the theory of B-scan imaging; for a sampler the reader is referred to [Fat80], [Fla81], [Fla83]. This technique is in wide use by the medical community and the reader's attention is drawn to the well-known book by Wells [Wel77] for an exhaustive treatment of the subject.

One of the first approaches to reflection tomography was by Johnson *et al.* [Joh78] who employed a ray tracing approach to synthetic aperture imaging. This approach attempts to correct for refraction and attenuation but ignores diffraction. In 1979, Norton and Linzer [Nor79a], [Nor79b] published a backprojection-based method for reconstructing ultrasonic reflectivity. A more rigorous treatment and a further generalization of this approach were then presented in [Nor81] where different possible scanning configurations were also discussed.

More recently, Dines [Din85] has shown experimental results that establish the feasibility of this imaging modality, although much work remains to be done for improving the quality of the reconstructed image. Also, recently, computer simulation results that show the usefulness of spectral extrapolation techniques to reflection tomography were presented in [Rob85].

8.6 References

[Din85] K. A. Dines, "Imaging of ultrasonic reflectivity," presented at the Symposium on Computers in Ultrasound, Philadelphia, PA, 1985.

[Fat80] M. Fatemi and A. C. Kak, "Ultrasonic B-scan imaging: Theory of image formation and a technique for restoration," *Ultrason. Imaging,* vol. 2, pp. 1–47, Jan. 1980.

[Fla81] S. W. Flax, G. H. Glover, and N. J. Pelc, "Textural variations in B-mode ultrasonography: A stochastic model," *Ultrason. Imaging,* vol. 3, pp. 235–257, 1981.

[Fla83] S. W. Flax, N. J. Pelc, G. H. Glover, F. D. Gutmann, and M. McLachlan, "Spectral characterization and attenuation measurements in ultrasound," *Ultrason. Imaging,* vol. 5, pp. 95–116, 1983.

[Ger74] G. Gerchberg, "Super-resolution through error energy reduction," *Opt. Acta,* vol. 21, pp. 709–720, 1974.

[Joh78] S. A. Johnson, J. F. Greenleaf, M. Tanaka, B. Rajagopalan, and R. C. Bahn,

"Quantitative synthetic aperture reflection imaging with correction for refraction and attenuation: Application of seismic techniques in medicine," presented at the San Diego Biomedical Symposium, San Diego, CA, 1978.

[Nor79a] S. J. Norton and M. Linzer, "Ultrasonic reflectivity tomography: Reconstruction with circular transducer arrays," *Ultrason. Imaging,* vol. 1, no. 2, pp. 154–184, Apr. 1979.

[Nor79b] ——, "Ultrasonic reflectivity tomography in three dimensions: Reconstruction with spherical transducer arrays," *Ultrason. Imaging,* vol. 1, no. 2, pp. 210–231, 1979.

[Nor81] ——, "Ultrasonic reflectivity imaging in three dimensions: Exact inverse scattering solutions for plane, cylindrical and spherical apertures," *IEEE Trans. Biomed. Eng.,* vol. BME-28, pp. 202–220, 1981.

[Pap75] A. Papoulis, "A new algorithm in spectral analysis and band limited extrapolation," *IEEE Trans. Circuits Syst.,* vol. CAS-22, pp. 735–742, Sept. 1975.

[Rob85] B. A. Roberts and A. C. Kak, "Reflection mode diffraction tomography," *Ultrason. Imaging,* vol. 7, pp. 300–320, 1985.

[Wel77] P. N. T. Wells, *Biomedical Ultrasonics.* London, England: Academic Press, 1977.